

Velocity continuation in the downward continuation approach to seismic imaging

Anton A. Duchkov and Maarten V. de Hoop

Center for Computational and Applied Mathematics, Purdue University, 150 N. University Street, West Lafayette IN 47907, USA.

E-mail: aduchkov@purdue.edu

Accepted 2008 October 23. Received 2008 October 16; in original form 2008 February 12

SUMMARY

One way of developing a wave-equation approach to seismic imaging is based on the concept of downward continuation of observed surface reflection data. Seismic imaging is typically based on the single scattering approximation, and assumes the knowledge of a smooth background model in which the mentioned downward continuation is carried out using the double-square-root (DSR) equation. The downward continued data are subjected, at each depth, to an imaging condition generating an image or to an angle transform generating common-image gathers. Motivated by the problem of estimation of the background model we develop a framework for velocity continuation in the downward continuation approach to seismic imaging. Velocity continuation is a term used to describe the transformation of a common-image gather (or image) obtained in an ‘initial’ background velocity model into a gather (image) obtained in another ‘final’ model. We construct evolution equations for velocity continuation. We then introduce the concept of data-extended-image ‘volume’. In the data-extended-image ‘volume’ we consider so-called extended images, which are functions of subsurface source–receiver midpoint, subsurface source–receiver offset and depth. We introduce and analyse velocity continuation of the individual components that make up the process of migration, imaging and the transformation to angle common-image gathers.

Key words: Controlled source seismology; Theoretical seismology; Wave propagation.

1 INTRODUCTION

In reflection seismology one places point sources and point receivers on or near the Earth’s surface. Each source generates waves in the subsurface, that are reflected where the medium properties vary discontinuously. The recorded reflections observed at the receivers (data) are used to create an image of these discontinuities or reflectors (Claerbout 1985; Biondi 2006). Seismic imaging is typically based on the single scattering approximation, and assumes the knowledge of a smooth background model. In reality, the background velocity model is not known and one can generate different images using the same data by making different assumptions about the model. This leads to the notion of velocity continuation, which was introduced by Fomel (1994) for homogeneous background models (see also Claerbout 1986). The concept of seismic image continuation was further developed in other works (Goldin 1994, 2003; Tygel *et al.* 1996; Hubral *et al.* 1996; Liu & McMechan 1996; Fomel 2003a; Iversen 1996; Adler 2002; Iversen 2006) including varying background media assuming the absence of caustics.

One way of developing a wave-equation approach to seismic imaging is based on the concept of downward continuation. In this paper, we consider downward continuation described by the double-square-root (DSR) equation (Belonosova & Alekseev 1967; Clayton 1978; Claerbout 1985), which is intimately connected to the one-way wave equation (Claerbout 1985; Fishman & McCoy 1984a,b). The key assumption for the constructions presented here to apply is the so-called DSR condition: The rays are nowhere horizontal, that is energy propagates nowhere horizontally. In our analysis, it is essential to consider so-called extended images and image gathers rather than traditional images. Velocity continuation is built from ‘invertible’ operators. A straightforward dimension check, in three dimensions, reveals that reflection seismic data (maximal acquisition geometry) are 5-D while a traditional image is 3-D. Indeed, the extension of the image while matching the dimensions of the data results in the required ‘invertibility’ (of the time-to-depth conversion operator Stolk & De Hoop 2006) even in the presence of caustics.

Extended images and common-image gathers reflect the redundancy in seismic data, and can be exploited in wave-equation reflection tomography or migration velocity analysis (MVA). In wave-equation MVA one aims at determining the background model using the reflections

in the data without knowing where the scatterers are. Typically, the reflection tomography is carried out through optimization (Symes & Carazzone 1991; Stolk & De Hoop 2001; Shen 2004; Sava & Biondi 2004; De Hoop *et al.* 2006) leading to a sequence of updates in the background model. Velocity continuation provides an efficient way of updating the extended image or common-image gathers, while sampling the background model space without remigrating the data. In homogeneous media, such a method—which is also referred to as residual migration—has been developed (Etgen 1990; Stolt 1996; Sava 2003). For heterogeneous media, ray perturbation theory (Farra 1999) has been used as a tool to construct velocity continuation ‘rays’ for the purpose of image continuation (Adler 2002; Iversen 2006).

The velocity continuation can, in all cases considered, be accomplished by solving an evolution equation (Duchkov *et al.* 2008a). The velocity continuation operator is the associated solution operator. It propagates singularities (‘fronts’) in accordance with ray theory associated with a Hamiltonian standardly obtained as the principal symbol of the evolution operator. The rays are sometimes referred to as velocity (continuation) rays. In the general case of heterogeneous background media, the calculation of the evolution operator generating the continuation does typically require retracing rays, dynamically, in changing models.

In this paper, we consider specifically velocity continuation through data downward continuation with the DSR equation. This allows an explicit construction of the underlying evolution equations that generate the velocity continuation. The evolution equations are defined on a 6-D data-extended-image ‘volume’ (for 3-D seismics). The usual coordinates for this volume are subsurface source–receiver midpoint, subsurface source–receiver offset, depth and two-way traveltime. Then surface data and an extended image (a function of subsurface source–receiver midpoint, offset and depth) appear to be defined on 5-D ‘hyperplanes’ in this ‘volume’. From this ‘volume’ one can also extract ‘virtual’ subsurface experiments that are defined on ‘hyperplanes’ corresponding to a constant depth. Common-image gathers are defined on a 5-D hypersurface. Velocity continuation can be applied to each of the components, generating these different quantities, that perform different tasks for background model, velocity, analysis.

First, we summarize the results of Duchkov *et al.* (2008a), which pertain to velocity continuation, in particular the existence of evolution equations driving the continuation (Section 2). In Section 3, we summarize data continuation in depth, making use of the DSR equations. In Section 4, we develop velocity continuation of downward continued data, using the DSR propagator, and construct the evolution equation and associated continuation rays in phase space. In Section 5, we introduce the velocity continuation of extended images, using a depth-to-time conversion operator, while in Section 6 we develop the velocity continuation of image gathers, using the so-called angle transform (Stolk & De Hoop 2001, 2006). The relevant derivations and constructions of evolution equations make use of Egorov’s theorem, which is described in Appendix A. Numerical examples, with a lens generating caustics in the background models and a horizontal reflector, of image continuation and continuation of image gathers are presented in Section 7. In Section 8, we construct evolution operators for the different types of velocity continuation in homogeneous velocity models in a closed form. These are used to illustrate the basic concepts, and recover, for example, the equations for residual Stolt migration (Stolt 1996). The Hamiltonian we construct here for velocity continuation of downward continuation reduces, in homogeneous models, to a form that is related to formulae obtained in (Fomel 2003a; Sava 2003). In Appendix B, we provide the evolution equations for velocity continuation of data downward continuation and extended image velocity continuation in background velocity models that vary in depth only, in particular the case of constant gradients.

2 PLATFORM FOR VELOCITY CONTINUATION

A comprehensive framework of continuation of seismic data and images was introduced in Duchkov *et al.* (2008a). Here, we summarize some key aspects of the theory developed there that apply to velocity continuation. To facilitate the introduction of velocity continuation, we consider a one-parameter family, $c(\alpha)$, of velocity models. This family can be viewed as a curve or trajectory in a space of allowable models. Optimization in wave-equation reflection tomography would yield samples of models on such a curve. Let $w(\alpha, X)$ denote downward continued data, an image or image gathers, evaluated with model $c(\alpha)$, whereas X stands for the coordinates of the space on which $w(\alpha, \cdot)$ is defined; α will be referred to as the evolution parameter.

Continuation operators. An operator $C_{(\alpha, \alpha_0)}$ is a continuation operator if it transforms $w(\alpha_0, \cdot)$ into $w(\alpha, \cdot)$, that is

$$C_{(\alpha, \alpha_0)} : w(\alpha_0, \cdot) \rightarrow w(\alpha, \cdot) \quad (1)$$

and satisfies the conditions

- $C_{(\alpha_0, \alpha_0)} = \mathbf{Id}$ identity operator;
- $C_{(\alpha, \alpha_0)}$ is invertible

for each $\alpha, \alpha \in J$, where $J = [\alpha_1, \alpha_2]$ is a given interval. In essence, properties (2) imply that $C_{(\alpha, \alpha_0)}$ is a propagator. Indeed, for $\alpha_0 \leq \alpha' \leq \alpha$ we have $C_{(\alpha, \alpha_0)} = C_{(\alpha, \alpha')}C_{(\alpha', \alpha_0)}$, and α mimics time as in wave propagation. The second condition in (2) states that the process of continuation can be reversed.

Evolution equation. With conditions (2) and some additional weak assumption (see Duchkov *et al.* 2008a), a continuation operator $C_{(\alpha, \alpha_0)}$ is the solution operator to an evolution equation, that is, $w(\alpha, \cdot) = C_{(\alpha, \alpha_0)}w(\alpha_0, \cdot)$ is the solution to the initial value problem

$$[\partial_\alpha - iP(\alpha, X, D_X)]w(\alpha, X) = 0, \quad w|_{\alpha=\alpha_0} = w(\alpha_0, \cdot), \quad (3)$$

where $D_X = -i\partial_X$ are differentiation operators with respect to coordinates X , in dimension n say. Sometimes, we will use the shorthand notation $P = P(\alpha)$. P is a pseudodifferential operator of order 1; the proof of its existence and a construction can be found in Duchkov *et al.*

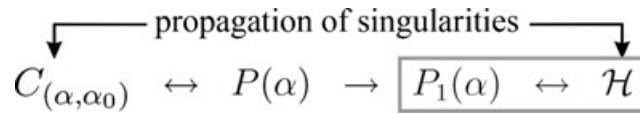


Figure 1. Propagation of singularities by the continuation operator (*cf.* 1) is governed by the evolution equation (*cf.* 3) via its principal symbol, and Hamiltonian (*cf.* 5).

(2008a). Basically, the action of \mathcal{Z} on w is given by

$$P(\alpha, X, D_X)w(\alpha, X) = \frac{1}{(2\pi)^n} \int P(\alpha, X, \Xi) e^{i(\Xi, X-Y)} w(\alpha, Y) dY d\Xi, \quad (4)$$

where $P(\alpha, X, \Xi)$ is the operator's symbol that is obtained from $P(\alpha, X, D_X)$ upon replacing D_X by Ξ . Certain mathematical details that pertain to velocity continuation with the DSR equation are omitted here; the DSR operator is not a pseudodifferential operator globally, but with the introduction of a judiciously chosen damping term, the methods developed here still apply.

Continuation rays. The solution operator of (3), that is the continuation operator, propagates singularities along rays in phase space. These rays are defined by the Hamiltonian,

$$H = H(\alpha, X, \xi_\alpha, \Xi) = \xi_\alpha - P_1(\alpha, X, \Xi), \quad (5)$$

where P_1 is the principal ('high-frequency') symbol of operator P . The Hamilton equations for generating the continuation rays are given by

$$\begin{aligned} \frac{dX}{d\alpha} &= \partial_\Xi H = -\partial_\Xi P_1, & \frac{d\Xi}{d\alpha} &= -\partial_X H = \partial_X P_1, \\ \frac{d\xi_\alpha}{d\alpha} &= -\partial_\alpha H = \partial_\alpha P_1, \end{aligned} \quad (6)$$

and are supplemented with initial conditions $X(\alpha_0) = X_0$, $\Xi(\alpha_0) = \Xi_0$, $\xi_\alpha(\alpha_0) = \xi_{\alpha_0}$. Note that the top equations do not depend on ξ_α and thus can be solved independently from the bottom equation. The solutions of (6) are also written as $X = X(\alpha, \alpha_0, X_0, \Xi_0)$, $\Xi = \Xi(\alpha, \alpha_0, X_0, \Xi_0)$, $\xi_\alpha = \xi_\alpha(\alpha, \alpha_0, X_0, \Xi_0, \xi_{\alpha_0})$.¹ A diagram emphasizing the interrelation between the continuation operator, the evolution operator and the underlying geometry and their high-frequency behaviour is given in Fig. 1.

In the case of image continuation, for example, the continuation operator can be naturally derived from the composition of a migration operator (in one model) with a demigration operator (in a variable model); for details, see section 4 of Duchkov *et al.* (2008a). Here, we address the construction of operators $P(\alpha, X, D_X)$ appearing in the velocity continuation of the components building the downward continuation approach to seismic imaging.

To facilitate the introduction of downward continuation, we write the coordinates in space as (z, x) , where z denotes depth and x the lateral coordinates. We will consider a family of background velocities, $c(\alpha) = c(\alpha; z, x)$. In practice, these will be defined by a representation in terms of basis functions with properties that are desirable (such as compression Loris *et al.* 2007) for the velocity analysis problem at hand.

3 DATA CONTINUATION IN DEPTH

In this section, we discuss operators for seismic data continuation derived from the DSR equation. The data are, implicitly, modelled in the single scattering approximation. We assume that the DSR assumption holds, that is energy propagates nowhere horizontally. Then the data can be modelled with the DSR equation. We consider data continuation in depth, z . The further analysis will be entirely based on the associated continuation operators. We reserve the symbol u for 'data'; u is a function of depth z , lateral source coordinates s , lateral receiver coordinates r and time t . Thus, $u(z = 0, s, r, t) = u_0(s, r, t)$ denotes observed reflection seismic data. The maximum depth considered is z_1 .

Upward continuation appears in the modelling of seismic reflection data (*cf.* Stolk & De Hoop 2005). The relevant initial value problem takes the form

$$(-\partial_z - iP^{DSR}(z, s, r, D_s, D_r, D_t))u = 0, \quad u(z_1, s, r, t) = u_1(s, r, t); \quad (7)$$

this equation is solved in the direction of decreasing z (upward, and forward in time) with initial condition defined at some large depth, z_1 say, at the bottom of the model. The DSR operator P^{DSR} has principal symbol,

$$P_1^{DSR}(z, s, r, \xi_s, \xi_r, \tau) = \tau \frac{1}{c(z, s)^2 - \frac{\|\xi_s\|^2}{\tau^2}} + \tau \frac{1}{c(z, r)^2 - \frac{\|\xi_r\|^2}{\tau^2}}, \quad (8)$$

while considering $\tau > 0$. Here, τ denotes frequency and ξ denotes horizontal wave vectors, ξ_s associated with s and ξ_r associated with r .

¹ In (Goldin 1998) continuation is formulated using notion of contact elements, which can be identified with $(X(\alpha, \alpha_0, X_0, \Xi_0), \Xi(\alpha, \alpha_0, X_0, \Xi_0)/\|\Xi(\alpha, \alpha_0, X_0, \Xi_0)\|)$ for each α . In image continuation, for example, $X(\alpha; X_0, \Xi_0)$ represents an image point corresponding with a reflector, while the direction of $\Xi(\alpha; X_0, \Xi_0)$ defines the normal to the reflector.

The upward continuation operator, $H_{(z,z_1)}^{\text{DSR}} \equiv C_{(z,z_1)}^{\text{DSR}}$, with $z < z_1$, is the solution operator of (7), that is, $u(z, \cdot) = H_{(z,z_1)} u_1$. (As compared with (3) we have $\alpha = z$ and $X = (s, r, t)$.) The adjoint, $H_{(0,z)}^*$, of $H_{(0,z)}$ appears to be a solution operator to the initial value problem,

$$[\partial_z - iP^{\text{DSR}}(z, s, r, D_s, D_r, D_t)]u = 0, \quad u(0, s, r, t) = u_0(s, r, t), \quad (9)$$

now to be solved in the direction of increasing z (downward, and backward in time) with initial condition defined at the surface. We have $u(z, \cdot) = H_{(0,z)}^* u_0$. We note that we have omitted non-selfadjoint contributions to P^{DSR} ; indeed, we have ignored evanescent waves. Then the following property holds true:

$$H_{(\bar{z},z)} H_{(\bar{z},z)}^* \sim \text{Id}. \quad (10)$$

We will substitute this composition while deriving different types of evolution operators for velocity continuation in the following sections. The DSR propagators are, microlocally, invertible.

Using (5), we obtain Hamiltonians for the DSR rays in phase space using depth as the evolution parameter

$$H^{\text{DSR}}(z, s, r, \xi_z, \xi_s, \xi_r, \tau) = \pm \xi_z - P_1^{\text{DSR}}(z, s, r, \xi_s, \xi_r, \tau), \quad (11)$$

in which the upper sign corresponds with downward continuation and the lower sign corresponds with upward continuation. Integrating the Hamilton equations (cf. 6) associated with upward continuation (cf. 7) yields solutions

$$(s(z, z_1, \Gamma_1), r(z, z_1, \Gamma_1), t(z, z_1, \Gamma_1), \xi_s(z, z_1, \Gamma_1), \xi_r(z, z_1, \Gamma_1), \tau(z, z_1, \Gamma_1)), \quad (12)$$

$$\Gamma_1 \equiv (s_1, r_1, t_1, \xi_{s1}, \xi_{r1}, \tau_1)$$

that define a mapping

$$\Sigma(z, z_1) : \Gamma_1 \rightarrow \underbrace{(s(z, z_1, \Gamma_1), r(z, z_1, \Gamma_1), t(z, z_1, \Gamma_1))}_{\Sigma_1(z, z_1)(\Gamma_1)} \underbrace{(\xi_s(z, z_1, \Gamma_1), \xi_r(z, z_1, \Gamma_1), \tau(z, z_1, \Gamma_1))}_{\Sigma_2(z, z_1)(\Gamma_1)}. \quad (13)$$

DSR rays are illustrated in Fig. 2. In Fig. 2(b) we show the usual way of describing a DSR ray as a pair of conventional rays connecting source and receiver locations at different depths (traveltime is implicit in this illustration). We note that, with $\xi_z = P_1^{\text{DSR}}(z, s, r, t, \xi_s, \xi_r, \tau)$, Σ also defines rays in $(z, s, r, t, \xi_s, \xi_r, \tau)$ -space. In Fig. 2(a) we illustrate the concept of data-extended-image volume, using coordinates (z, s, r, t) . A DSR ray is a curve in this volume. Through continuation in depth we sweep the data-extended-image volume with ‘virtual’ subsurface data sets.

The DSR assumption implies that (two-way) traveltime depends monotonically on depth. Also, for given (z, s, r, ξ_s, ξ_r) , the equation $H^{\text{DSR}}(z, s, r, \xi_z, \xi_s, \xi_r, \tau) = 0$ (cf. 11) can be solved for τ to yield a mapping $\Theta : \tau \rightarrow \xi_z = P_1^{\text{DSR}}(z, s, r, \xi_s, \xi_r, \tau)$; that is,

$$H^{\text{DSR}}(z, s, r, \Theta(z, s, r, \xi_s, \xi_r, \tau), \xi_s, \xi_r, \tau) = 0. \quad (14)$$

Then Θ^{-1} is the mapping that solves the equation (cf. 11)

$$\xi_z = P_1^{\text{DSR}}(z, s, r, \xi_s, \xi_r, \Theta^{-1}(z, s, r, \xi_z, \xi_s, \xi_r)) \quad (15)$$

(Stolk & De Hoop 2005, lemma 4.1).

In the further analysis, it appears useful to transform coordinates from subsurface lateral source and receiver to subsurface midpoint and offset,

$$x = \frac{1}{2}(r + s), \quad h = \frac{1}{2}(r - s); \quad (16)$$

with the transformation

$$\xi_s = \frac{1}{2}(\xi_x - \xi_h), \quad \xi_r = \frac{1}{2}(\xi_x + \xi_h). \quad (17)$$

The DSR operator symbol is subjected to this coordinate transform to yield

$$P^{\text{DSR}}(z, x, h, \xi_x, \xi_h, \tau) = P^{\text{DSR}}(z, s(x, h), r(x, h), \xi_s(\xi_x, \xi_h), \xi_r(\xi_x, \xi_h), \tau). \quad (18)$$

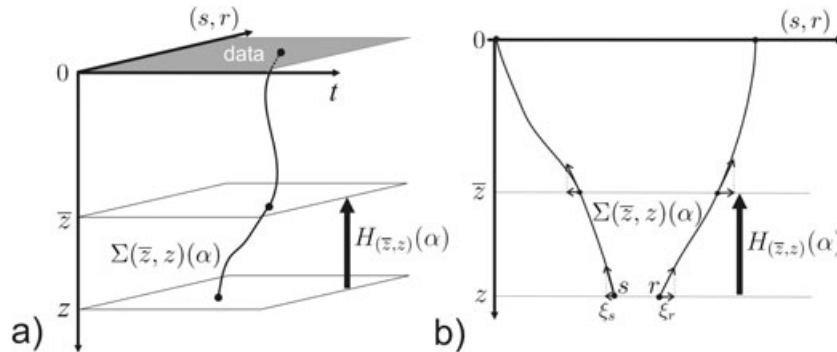


Figure 2. Geometry of upward data continuation operator. (a) The transformation Σ and a DSR ray in the data-extended-image volume; (b) the transformation Σ and a DSR ray viewed as a pair of conventional rays.

REMARK (offset plane waves). We consider the situation where ξ_h is preserved along all DSR rays, that is $\frac{d\xi_h}{dz} = 0$ along these rays. This holds, in particular, in the case of a vertically inhomogeneous medium, $c = c(z)$. We downward continue, in such a $c(z)$ background model, independently every subset of the data corresponding to a constant value of ξ_h

$$[\partial_z - iP^{\text{DSR}}(z, x, h, D_x, \xi_h, D_t)]\hat{u} = 0, \quad \hat{u}(z, x, \xi_h, t)|_{z=0} = \hat{u}_0(x, \xi_h, t), \quad (19)$$

cf. (18), where \hat{u} denotes the Fourier transform of u with respect to h . The principal symbol of the evolution operator can be written in the form (cf. 11 subject to coordinate transformation 16–17):

$$P_1^{\text{DSR}}(z, x, h, \xi_x, \xi_h, \tau) = \tau \frac{1}{b(z)^2} - \frac{\|\xi_x\|^2 + 2\langle \xi_h, \xi_x \rangle}{\tau^2} + \tau \frac{1}{b(z)^2} - \frac{\|\xi_x\|^2 - 2\langle \xi_h, \xi_x \rangle}{\tau^2}, \quad (20)$$

in which $b(z)^{-2} = c(z)^{-2} - \|\xi_h\|^2 \tau^{-2}$. The operator with principal symbol (20) was introduced in Foster *et al.* (2002) for so-called pre-stack offset plane wave migration. If the term, $2\langle \xi_h, \xi_x \rangle$, is omitted, then the operator in (20) reduces to a zero (source–receiver) offset migration, with modified velocity given by $b(z)$, for each ξ_h (Mosher *et al.* 1996).

4 VELOCITY CONTINUATION OF DOWNWARD CONTINUED DATA

4.1 Data downward continuation

In this section, we apply the notion of velocity continuation to data downward continuation. To this end, we reconsider the smooth family of background velocity models, $c(\alpha; z, x)$, depending on a parameter α . The initial value problem (9) for downward continuation is modified to depend smoothly on α

$$[\partial_z - iP^{\text{DSR}}(\alpha; z, s, r, D_s, D_r, D_t)]u(\alpha; \cdot) = 0, \quad u(\alpha; 0, s, r, t) = u_0(s, r, t), \quad (21)$$

in which the principal symbols of the one-parameter family of DSR operators,

$$P^{\text{DSR}}(\alpha) = P^{\text{DSR}}(\alpha; z, s, r, D_s, D_r, D_t),$$

are given by

$$P_1^{\text{DSR}}(\alpha; z, s, r, \xi_s, \xi_r, \tau) = \tau \frac{1}{c(\alpha; z, s)^2} - \frac{\|\xi_s\|^2}{\tau^2} + \tau \frac{1}{c(\alpha; z, r)^2} - \frac{\|\xi_r\|^2}{\tau^2} \quad (22)$$

and is solved in the direction of increasing z as before. Naturally, surface reflection data, u_0 , are assumed to be independent of α . (However, one could account for α -dependent data in time-lapse seismic surveys). Here, the solution $u(\alpha; z, s, r, t)$ corresponds with data downward continued from the surface ($z = 0$) to depth z assuming a background velocity model $c(\alpha; z, x)$.

4.2 Construction of the velocity continuation operator

To develop an operator for continuing $u(\alpha; z, s, r, t)$ in α , we will need $\partial_\alpha P^{\text{DSR}}$, which is still essentially a pseudodifferential operator of order 1. The principal symbol of $\partial_\alpha P^{\text{DSR}}$ is given by

$$\partial_\alpha P^{\text{DSR}}_1(\alpha; z, s, r, \xi_s, \xi_r, \tau) = -\mathbf{p} \frac{\tau}{c_s^{-2} - \|\xi_s\|^2/\tau^2} \frac{\partial_\alpha c_s}{c_s^3} - \mathbf{p} \frac{\tau}{c_r^{-2} - \|\xi_r\|^2/\tau^2} \frac{\partial_\alpha c_r}{c_r^3}, \quad (23)$$

in which $c_s = c(\alpha; z, s)$, and $c_r = c(\alpha; z, r)$.

A family of velocity models, $c(\alpha; z, x)$, induces a family of solution operators, $H_{(0,z)}^*(\alpha)$, to the initial value problems (21), that is, $u(\alpha; z, s, r, t) = H_{(0,z)}^*(\alpha) u_0$. The velocity continuation of $u(\alpha; z, s, r, t)$, that is data downward continued to a given depth z , is described by the continuation operator,

$$C_{(\alpha, \alpha_0)}^d(z) = H_{(0,z)}^*(\alpha) H_{(0,z)}(\alpha_0). \quad (24)$$

From the properties of $H_{(0,z)}(\alpha)$ (Stolk & De Hoop 2006) it indeed follows that condition (2) is satisfied. Then

$$u(\alpha; z, \cdot) = C_{(\alpha, \alpha_0)}^d(z) u(\alpha_0; z, \cdot).$$

The action of the continuation operator defined in (24) is illustrated in Fig. 3, while showing the geometry of the associated operator composition, both in the data-extended-image volume and as a pair of source–receiver rays.

In accordance with the theory summarized in Section 2, $C_{(\alpha, \alpha_0)}^d(z)$ is the solution operator to an evolution equation,

$$[\partial_z - iP^d(\alpha)]u(\alpha; z, \cdot) = 0, \quad u(\alpha_0; z, \cdot) = H_{(0,z)}^*(\alpha_0) u_0(\cdot), \quad (25)$$

for each z ; the (principal) symbol of $P^d(\alpha)$ is constructed below. With (24) we find that $iP^d(\alpha) = (\partial_\alpha H_{(0,z)}^*)(\alpha) H_{(0,z)}(\alpha)$. As before, we have assumed that the surface reflection data u_0 are independent of α . (As compared with (3) we have $X = (s, r, t)$; z has become a parameter.)

Upon substituting $u(\alpha; z, \cdot)$ in (25) into (21), and taking a formal derivative with respect to α , we obtain

$$[\partial_z - iP^{\text{DSR}}(\alpha)] \partial_\alpha H_{(0,z)}^*(\alpha) u_0 = i \partial_\alpha P^{\text{DSR}}(\alpha) H_{(0,z)}^*(\alpha) u_0. \quad (26)$$

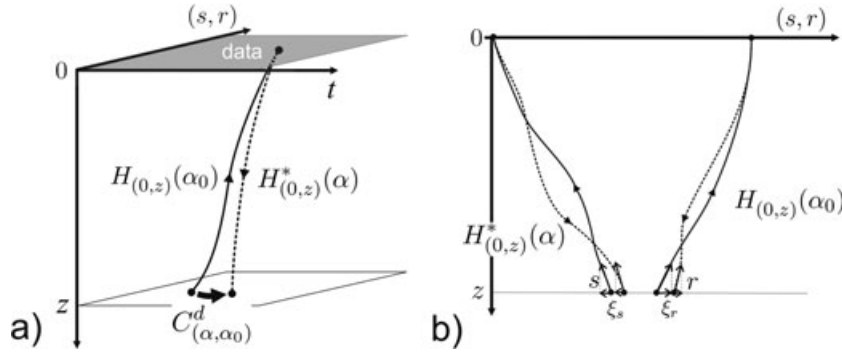


Figure 3. Continuation of the downward continued data (cf. (24)) as a composition of operators: (a) geometry in the data-extended-image volume (using DSR rays); (b) geometry for a pair of source–receiver rays.

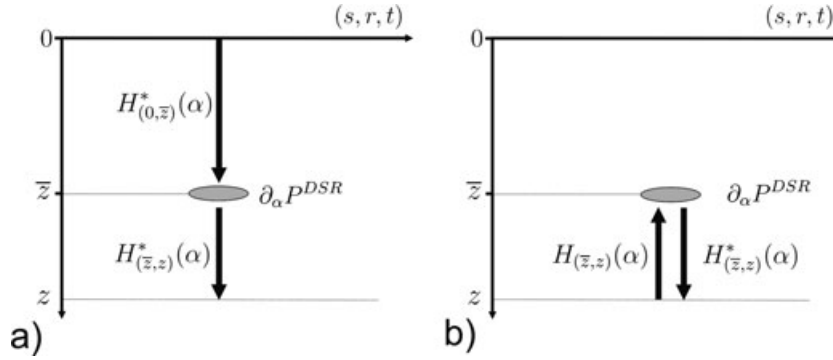


Figure 4. Calculation of velocity continuation of downward continued data. Linear perturbation due to smooth variations of the background velocity (a) as manifestation of transmission tomography (cf. 27) and (b) as manifestation of reflection tomography (cf. 28).

Eq. (26) is an inhomogeneous variant of eq. (21) satisfied by the function $\partial_\alpha H_{(z,0)}^*(\alpha)u_0$. Its solution may be expressed in the form

$$\partial_\alpha H_{(0,z)}^*(\alpha)u_0(z, \cdot) = i \int_0^z H_{(\bar{z},z)}^*(\alpha) \partial_\alpha P^{DSR}(\alpha) H_{(0,\bar{z})}^*(\alpha) d\bar{z} u_0. \quad (27)$$

This equation is identical to eq. (C4) in De Hoop *et al.* (2006) (but without the pseudodifferential factors \mathcal{Q} and microlocal cut-offs ψ).

Furthermore, we can rewrite (27) in the form

$$\partial_\alpha H_{(0,z)}^*(\alpha)u_0 = iP^d(\alpha)H_{(0,z)}^*(\alpha)u_0, \quad P^d(\alpha) = \int_0^z H_{(\bar{z},z)}^*(\alpha) \partial_\alpha P^{DSR}(\alpha) H_{(\bar{z},z)}(\alpha) d\bar{z}, \quad (28)$$

where we used the properties that $H_{(\bar{z},z)}(\alpha)H_{(\bar{z},z)}^*(\alpha) \sim Id$ and $H_{(0,z)}^*(\alpha) = H_{(\bar{z},z)}^*(\alpha)H_{(0,\bar{z})}^*(\alpha)$ with $0 < \bar{z} < z$. We note that expressions (27) and (28) provide two ways of calculating the perturbation of downward continued data, $u(\alpha; z, s, r, t) = H_{(0,z)}^*(\alpha)u_0$ (at depth z) due to smooth perturbations of background velocities. Both ways are illustrated schematically in Fig. 4. The evaluation of the integrand in the integral on the right-hand side of (27), for one fixed \bar{z} , is illustrated in Fig. 4(a). This formulation mimics transmission tomography (with the DSR equation) as it connects surface data to downward continued data adding up perturbation contributions on the way. The evaluation of the integrand (for one fixed \bar{z}) in the integral representation for $P^d(\alpha)$ (28) is illustrated in Fig. 4(b). The scheme follows the cascading of upward and downward continuation operators. This approach fits the concept of velocity continuation as it acts on downward continued data $u(\alpha; z, s, r, t)$ while its output is again u subject to a background velocity perturbation. This description is naturally connected with reflection tomography.

According to Egorov's theorem (see Appendix A), $\mathcal{Q}^d(\alpha; \bar{z}, z) = H_{(\bar{z},z)}^*(\alpha)(\partial_\alpha P^{DSR}(\alpha))H_{(\bar{z},z)}(\alpha)$ is a pseudodifferential operator of order 1, the principal symbol of which is obtained by the transformation

$$\mathcal{Q}_1^d(\alpha; \bar{z}, z, s, r, t, \xi_s, \xi_r, \tau) = \partial_\alpha P^{DSR}_1(\alpha; \bar{z}, \Sigma'(\bar{z}, z)(s, r, t, \xi_s, \xi_r, \tau)), \quad (29)$$

with $\bar{z} < z$. Σ is the transformation describing upward DSR rays in phase space in velocity model $c(\alpha; z, x)$, while the explicit expression for $(\partial_\alpha P^{DSR})_1$ was given in (23); the prime in Σ' indicates that the output time coordinate in Σ (cf. 13) has been removed (since P_1^{DSR} does not depend on t). We obtain

$$P_1^d(\alpha; z, s, r, t, \xi_s, \xi_r, \tau) = \int_0^z \mathcal{Q}_1^d(\alpha; \bar{z}, z, s, r, t, \xi_s, \xi_r, \tau) d\bar{z}. \quad (30)$$

The Hamiltonian associated with (25) is given by

$$H^d(\alpha; z, s, r, \xi_s, \xi_r, \tau) = \xi_\alpha - P_1^d(\alpha; z, s, r, \xi_s, \xi_r, \tau). \quad (31)$$

The Hamilton equations (cf. 6) that generate the continuation rays take the form

$$\begin{aligned}\frac{d(s, r, t)}{d\alpha} &= -\frac{\partial P_1^d}{\partial(\xi_s, \xi_r, \tau)} = V_1(\alpha, z; s, r, t, \xi_s, \xi_r, \tau), \\ \frac{d(\xi_s, \xi_r, \tau)}{d\alpha} &= \frac{\partial P_1^d}{\partial(s, r, t)} = V_2(\alpha, z; s, r, t, \xi_s, \xi_r, \tau),\end{aligned}\quad (32)$$

in which

$$V_1(\alpha, z; \cdot) = -\int_0^z \frac{\partial \Sigma_1(\bar{z}, z)}{\partial(\xi_s, \xi_r, \tau)} \frac{\partial \square P^{\text{DSR}}}{\partial(s, r, t)}(\alpha; z, \Sigma'(\bar{z}, z)(\cdot)) + \frac{\partial \Sigma_2(\bar{z}, z)}{\partial(\xi_s, \xi_r, \tau)} \frac{\partial \square P^{\text{DSR}}}{\partial(\xi_s, \xi_r, \tau)}(\alpha; z, \Sigma'(\bar{z}, z)(\cdot)) d\bar{z}, \quad (33)$$

$$V_2(\alpha, z; \cdot) = \int_0^z \frac{\partial \Sigma_1(\bar{z}, z)}{\partial(s, r, t)} \frac{\partial \square P^{\text{DSR}}}{\partial(s, r, t)}(\alpha; z, \Sigma'(\bar{z}, z)(\cdot)) + \frac{\partial \Sigma_2(\bar{z}, z)}{\partial(s, r, t)} \frac{\partial \square P^{\text{DSR}}}{\partial(\xi_s, \xi_r, \tau)}(\alpha; z, \Sigma'(\bar{z}, z)(\cdot)) d\bar{z}; \quad (34)$$

here, the derivatives in $\frac{\partial \Sigma_{1,2}(\bar{z}, z)}{\partial(s, r, t)}$, $\frac{\partial \Sigma_{1,2}(\bar{z}, z)}{\partial(\xi_s, \xi_r, \tau)}$ follow ray perturbations (with respect to initial parameters) calculated along the unperturbed DSR rays (cf. 12). Indeed, we have followed a linear perturbation argument much in the spirit of ray perturbation theory (Farra 1999). The formulae are different from the ones in the direct extension approach of Iversen (2006), however, as he does not construct the continuation Hamiltonian.

5 VELOCITY CONTINUATION OF EXTENDED IMAGES

Migration with the DSR equation is designed around downward continuation of the data into the subsurface, which is followed by applying appropriate imaging conditions: Restricting for each depth the downward continued data to $t = 0$ and $s = r = x$. However, here, we are interested in applying only the first imaging condition leading to an extended image, $w_e(z, s, r)$, say (note that s and r represent *subsurface* source and receiver coordinates). This object is relevant, for example, for developing tools for MVA; see also the next subsection. (A usual image, at (z, x) , is obtained as $w_e(z, x, x)$.)

5.1 Depth-to-time conversion operator

Modelling. Seismic reflection data, in Born approximation, can be modelled with an inhomogeneous DSR equation (Stolk & De Hoop 2005):

$$(-\partial_z - iP^{\text{DSR}}(z, s, r, D_s, D_r, D_t)) u = R(z, s, r, t), \quad u|_{z=z_1} = 0, \quad (35)$$

where

$$R(z, s, r, t) = \delta(t)\delta(r-s)\frac{1}{2}(c^{-3}\delta c)\left(z, \frac{1}{2}(r+s)\right); \quad (36)$$

$\delta c(z, x)$ is the function containing the rapid velocity variations representative of the scatterers, superimposed on a smooth background model $c(z, x)$ (which will be parametrized by α). The data are then modelled by the solution at $z = 0$: $u(z = 0, s, r, t)$.

Let R_t denote the restriction to $t = 0$ (that is, setting t equal to zero) and $E_t = R_t^*$ its adjoint (that is, multiplication by $\delta(t)$). In the above, $\delta(r-s)\frac{1}{2}(c^{-3}\delta c)(z, \frac{1}{2}(r+s))$ represents the contrast in ‘image’ space, which, if subjected to E_t , gives $R(z, s, r, t)$ in (36). An extended image follows from the surface reflection data, u_0 , as

$$w_e(\alpha; z, \cdot) = N(\alpha)^{-1} R_t H_{(0,z)}^*(\alpha) u_0, \quad (37)$$

where $N(\alpha)$ is a pseudodifferential operator correcting for ‘amplitudes’ and illumination, using a background velocity model parametrized by α as before. We identify $R_t H_{(0,z)}^*(\alpha)$ with the adjoint, $K^*(\alpha)$, of an operator $K(\alpha)$, with

$$u_0 = K(\alpha) w_e(\alpha; \cdot) = \int_0^{z_1} H_{(0,\bar{z})}(\alpha) E_t w_e(\alpha; \bar{z}, \cdot) d\bar{z}, \quad (38)$$

while $N(\alpha) = K^*(\alpha) K(\alpha)$ and has a parametrix, $N(\alpha)^{-1}$. In Stolk & De Hoop (2006), it was established that $K(\alpha)$ is (microlocally) invertible. Up to the differentiation $[-\frac{1}{2}\partial_t^2]$ the operator K corresponds with the depth-to-time conversion operator \tilde{K} in Stolk & De Hoop (2006). The canonical transformation associated with $K(\alpha)$ is given by theorem 4.2 of Stolk & De Hoop (2005)

$$\Sigma_K : (z, s, r, \xi_s, \xi_r) \rightarrow \Sigma(0, z)(s, r, 0, \xi_s, \xi_r, \Theta^{-1}(z, s, r, \xi_s, \xi_r)). \quad (39)$$

It is illustrated in Fig. 5(a). Compared with downward continuation (see Fig. 2a) one traces DSR rays in the data-extended-image volume until two-way traveltimes becomes zero.

5.2 Construction of the velocity continuation operator

The velocity continuation of an extended image is described by

$$w_e(\alpha; \cdot) = C_{(\alpha, \alpha_0)}^e w_e(\alpha_0; \cdot), \quad (40)$$

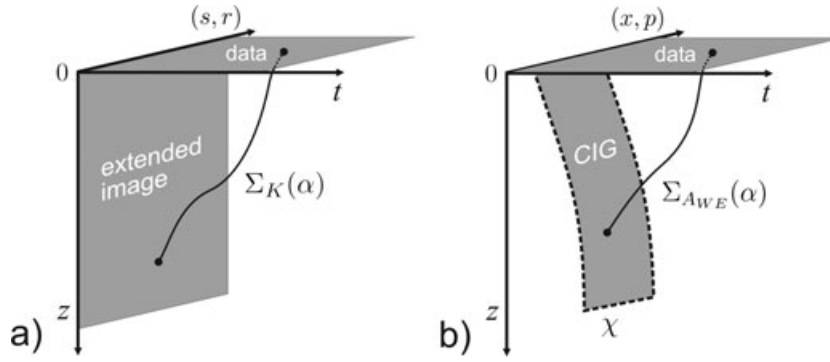


Figure 5. Illustration of canonical transformations (a) for depth-to-time conversion operator, $K(\alpha)$, relating data to an extended image, and (b) for wave-equation angle transform $A_{WE}(\alpha)$ relating data to common-image gathers.

where $C_{(\alpha, \alpha_0)}^e$ denotes the relevant continuation operator. Using the depth-to-time conversion operator concept, we get

$$C_{(\alpha, \alpha_0)}^e w_e(\alpha_0; \cdot) = N(\alpha)^{-1} K^*(\alpha) K(\alpha_0) w_e(\alpha_0; \cdot). \quad (41)$$

With the properties of $K(\alpha_0)$ (Stolk & De Hoop 2006, section 2), it follows that condition (2) is satisfied. Then we construct an evolution equation for $w_e(\alpha)$ with respect to α . Differentiation of $C_{(\alpha, \alpha_0)}^e w_e(\alpha_0; \cdot)$ in (41) with respect to α yields two terms: The term,

$$\partial_\alpha N^{-1}(\alpha) N(\alpha) C_{(\alpha, \alpha_0)}^e w_e(\alpha_0; \cdot),$$

is of order zero, and is neglected in the further analysis. The leading order (order one) term gives

$$iN^{-1}(\alpha) R_t P^d(\alpha) H_{(0,z)}^*(\alpha) K(\alpha_0) w_e(\alpha_0; \cdot), \quad (42)$$

upon substituting (28). This operator, using (10), can be rewritten as

$$iN^{-1}(\alpha) K^*(\alpha) H_{(0,z)}(\alpha) P^d(\alpha) H_{(0,z)}^*(\alpha) K(\alpha) C_{(\alpha, \alpha_0)}^e = iP^e(\alpha) C_{(\alpha, \alpha_0)}^e. \quad (43)$$

We apply Egorov's theorem twice, and find that $P^e(\alpha)$ is a pseudodifferential operator the principal symbol of which is obtained from the principal symbol of $P^d(\alpha)$ via two successive transformations of variables: The transformation associated with $H_{(0,z)}(\alpha)$ is $\Sigma(0, z)$ given in (13) with $z = 0$ and $z_1 = z$, while the transformation associated with $K(\alpha)$ is Σ_K given in (39). The composition of transformations then yields

$$\Sigma(z, 0) \circ \Sigma_K : (z, s, r, \xi_z, \xi_s, \xi_r) \rightarrow (0, s, r, \xi_s, \xi_r, \Theta^{-1}(z, s, r, \xi_z, \xi_s, \xi_r)), \quad (44)$$

which appears in the application of Egorov's theorem (see Appendix A) to (43). We get

$$P_1^e(\alpha; z, s, r, \xi_z, \xi_s, \xi_r) = P_1^d(\alpha; z, s, r, \xi_s, \xi_r, \Theta^{-1}(z, s, r, \xi_z, \xi_s, \xi_r)) \quad (45)$$

up to principal parts. $C_{(\alpha, \alpha_0)}^e$ is the solution operator associated with the evolution equation,

$$\partial_\alpha - iP^e(\alpha) w_e(\alpha; \cdot) = 0. \quad (46)$$

(As compared with (3) we have $X = (z, s, r)$.) The corresponding Hamiltonian becomes

$$H^e(\alpha; z, s, r, \xi_z, \xi_s, \xi_r) = \xi_\alpha - P_1^e(\alpha; z, s, r, \xi_z, \xi_s, \xi_r). \quad (47)$$

In general, the evaluation of symbols $P_1^d(\alpha; z, s, r, \xi_s, \xi_r, \tau)$ and $P_1^e(\alpha; z, s, r, \xi_z, \xi_s, \xi_r)$ (cf. 45) requires retracing DSR rays for each α (cf. 29–30). However, in the special case of vertically inhomogeneous background velocities, this can be avoided, see Appendix B.

6 VELOCITY CONTINUATION OF IMAGE GATHERS

Surface reflection data are, formally, redundant: The measurements are taken in $2n - 1$ variables, while the image to be constructed is a function of n variables. This redundancy can be used in wave-equation MVA (Symes & Carazzone 1991; Stolk & De Hoop 2001; Shen 2004; Sava & Biondi 2004; De Hoop *et al.* 2006) analysing so-called common-image gathers (for a discussion on various types of common-image gathers, see Biondi (2006)).

The redundancy is revealed, even in the presence of caustics, by the angle transform, A_{WE} , as defined in Stolk & De Hoop (2001, 2006), which generates 'angle' common-image gathers, here denoted by w_g , from surface reflection data, u_0 . Here, we consider the velocity continuation of these image gathers, with velocity models $c = c(\alpha; z, x)$ parametrized by α as before.

6.1 Wave-equation angle transform

Let $A_{WE}(\alpha)$ denote a family of angle transforms parametrized by α ; $A_{WE}(\alpha)$ is defined by

$$w_g(\alpha) = A_{WE}(\alpha)u_0 = B\chi H_{(0,z)}^*(\alpha)u_0, \quad \text{with} \quad B\chi : u(z, s, r, t) \rightarrow (B\chi u)(z, x, p) = u(z, x - h, x + h, \langle p, 2h \rangle)\chi(z, x, h)dh, \quad (48)$$

in which $\chi(z, x, h)$ is a taper function attaining the value 1 about $h = 0$ (which ensures that the image gather is artefact free in the presence of caustics); here, (z, x) are the coordinates of an image point. (A conventional common-image gather is $w_g(\alpha; z, x, p)$ as a function of (z, p) for fixed x .) We note that p is a $(2n - 1 - n = n - 1)$ -dimensional (co)vector, and can be connected to scattering angle and azimuth associated with the geometry of reflected rays (De Hoop *et al.* 2003).

The angle transform is (microlocally) invertible (Stolk & De Hoop 2006). The canonical transformation associated with A_{WE}^{-1} is given by

$$\Sigma_{A_{WE}}^{-1} : (z, x, p, \xi_z, \xi_x, \xi_p) \rightarrow \Gamma_A = (s_0, r_0, t_0, \xi_{s0}, \xi_{r0}, \tau), \quad (49)$$

where Γ_A is the solution of the system of equations (Stolk & De Hoop 2006, theorem. 3.1):

$$\begin{aligned} P_1^{\text{DSR}}(z, s(z, 0, \Gamma_A), r(z, 0, \Gamma_A), \xi_s(z, 0, \Gamma_A), \xi_r(z, 0, \Gamma_A), \tau) &\stackrel{*}{=} \xi_z, \\ \frac{1}{2}[s(z, 0, \Gamma_A) + r(z, 0, \Gamma_A)] &= x, \quad \xi_s(z, 0, \Gamma_A) = \frac{1}{2}\xi_x + \tau p, \\ \tau[r(z, 0, \Gamma_A) - s(z, 0, \Gamma_A)] &= \xi_p, \quad \xi_r(z, 0, \Gamma_A) = \frac{1}{2}\xi_x - \tau p; \end{aligned} \quad (50)$$

the solution is constrained by the equation

$$\tau^{-1} \square (\xi_s(z, 0, \Gamma_A) - \xi_r(z, 0, \Gamma_A)), r(z, 0, \Gamma_A) - s(z, 0, \Gamma_A) \square = t(z, 0, \Gamma_A) \quad (51)$$

for each z ; cf. 13. The equation labelled with $*$ can be rewritten as

$$\Theta^{-1}(z, s(z, 0, \Gamma_A), r(z, 0, \Gamma_A), \xi_z, \xi_s(z, 0, \Gamma_A), \xi_r(z, 0, \Gamma_A)) = \tau. \quad (52)$$

In Fig. 5(b) we illustrate the canonical relation for the wave-equation angle transform. The region surrounded by a dashed line illustrates the fact that the invertibility of $A_{WE}(\alpha)$ holds microlocally subject to a cut-off provided by the window function $\chi(z, x, h)$ in (48).

6.2 Construction of the velocity continuation operator

The velocity continuation of image gathers is described by

$$w_g(\alpha; z, x, p) = C_{(\alpha, \alpha_0)}^g w_g(\alpha_0; z, x, p), \quad (53)$$

where $C_{(\alpha, \alpha_0)}^g$ denotes the relevant continuation operator. Using that the angle transform is (microlocally) invertible, we have

$$C_{(\alpha, \alpha_0)}^g = A_{WE}(\alpha)A_{WE}^{-1}(\alpha_0). \quad (54)$$

With the properties of A_{WE}^{-1} (Stolk & De Hoop 2006, section 3), condition (2) is satisfied. We now construct an evolution equation for $w_g(\alpha; \cdot)$ with respect to α .

Differentiation of $C_{(\alpha, \alpha_0)}^g w_g(\alpha_0; \cdot)$ in (53) with respect to α yields

$$\partial_\alpha C_{(\alpha, \alpha_0)}^g w_g(\alpha_0; \cdot) = iB\chi P^d(\alpha)H_{(0,z)}^*(\alpha)A_{WE}^{-1}(\alpha_0)w_g(\alpha_0; \cdot), \quad (55)$$

upon substituting (28). We can rewrite the composition of operators acting on $w_g(\alpha_0; \cdot)$ on the right-hand side in the form

$$iA_{WE}(\alpha)H_{(0,z)}(\alpha)P^d(\alpha)H_{(0,z)}^*(\alpha)A_{WE}^{-1}(\alpha)C_{(\alpha, \alpha_0)}^g = iP^g(\alpha)C_{(\alpha, \alpha_0)}^g. \quad (56)$$

We apply Egorov's theorem twice, and find that $P^g(\alpha)$ is a pseudodifferential operator the principal symbol of which is obtained from the principal symbol of $P^d(\alpha)$ via two successive transformations of variables: The transformation associated with $H_{(0,z)}^*(\alpha)$ is $\Sigma(z, 0)$ given in (13) with $z_1 = 0$, while the transformation associated with $A_{WE}^{-1}(\alpha)$ is $\Sigma_{A_{WE}}^{-1}$ described in (49)–(52). The composition of these transformations is given by

$$\tilde{\Sigma} = \Sigma(z, 0) \circ \Sigma_{A_{WE}}^{-1} : (z, x, p, \xi_z, \xi_x, \xi_p) \rightarrow \Sigma(z, 0)(\Gamma_A) = \Gamma_B. \quad (57)$$

We note that Γ_A becomes implicit in this mapping; in fact, (50) and (51) constrain the elements of Γ_B . Due to the invertibility of $\Sigma(z, 0)$ (cf. 13), whence the canonical transformation associated with $A_{WE}^{-1}(\alpha)$ can be rewritten as

$$\Sigma_{A_{WE}}^{-1} : (z, x, p, \xi_z, \xi_x, \xi_p) \rightarrow \Gamma_A = \Sigma(0, z)(\Gamma_B), \quad (58)$$

it follows that s, r, ξ_s, ξ_r, τ in Γ_B solve the equations

$$\begin{aligned} \frac{1}{2}[s + r] &= x, \quad \xi_s = \frac{1}{2}\xi_x + \Theta^{-1}(z, s, r, \xi_z, \xi_s, \xi_r)p, \\ \Theta^{-1}(z, s, r, \xi_z, \xi_s, \xi_r)[r - s] &= \xi_p, \quad \xi_r = \frac{1}{2}\xi_x - \Theta^{-1}(z, s, r, \xi_z, \xi_s, \xi_r)p, \end{aligned} \quad (59)$$

while t follows from (51).

The composition in (57) appears in the application of Egorov's theorem (see Appendix A) to (56). We get:

$$P_1^g(\alpha; z, x, p, \xi_z, \xi_x, \xi_p) = P_1^d(\alpha; \tilde{\Sigma}'(z, x, p, \xi_z, \xi_x, \xi_p)); \quad (60)$$

as before, the prime in $\tilde{\Sigma}'$ indicates that the output time coordinate in $\tilde{\Sigma}$ has been removed. $C_{(\alpha, \alpha_0)}^g$ is the solution operator associated with the evolution equation,

$$\partial_\alpha - iP^g(\alpha) w_g(\alpha; \cdot) = 0. \quad (61)$$

(As compared with (3) we have $X = (z, x, p)$.) The corresponding Hamiltonian becomes

$$H^g(\alpha; z, x, p, \xi_\alpha, \xi_z, \xi_x, \xi_p) = \xi_\alpha - P_1^g(\alpha; z, x, p, \xi_z, \xi_x, \xi_p). \quad (62)$$

7 AN EXAMPLE: VELOCITY CONTINUATION WITH A LENS

In this section, we present a 2-D example of velocity continuation of common-image gathers, and of an extended image. We focus on the high-frequency aspects, carry out our calculations with the relevant principal symbols and follow the geometry of ‘fronts’ (singular supports to be precise). We specifically include the formation of caustics and illustrate that their presence is allowed in the approach developed here. We make use of background velocity models containing a low velocity lens

$$c(\alpha; x, z) = 1 - \alpha \exp[-7.5(x^2 + (1 - z)^2)], \quad (63)$$

where α defines the ‘strength’ of the lens. We take $\alpha = 0.2$ as our ‘true’ model (see Fig. 6a, where the smooth background velocity (low-velocity lens) is shown in grey scale). We consider a single, horizontal, reflector (solid line) at depth $z = 2$. Synthetic data, u_0 (traveltimes, as we consider only geometry), were generated in the ‘true’ model by methods of ray tracing. In Fig. 7, we show incident (a) and reflected (b) rays for one source position, to illustrate that in our example the DSR condition is satisfied, while caustics are being formed due to the lens.

In Fig. 6(b) we show a common-image gather (its singular support) $w_g = w_g(\alpha = 0.2; z, x, p)$ (cf. 48) if the ‘true’ background velocity model were used in the downward continuation. The reflector (the horizontal line in Fig. 6a) is mapped into a plane (Fig. 6b, in grey). A common-image gather is usually associated with an $x = \text{const}$ section (line 2); a constant p section corresponds to an image (line 1).

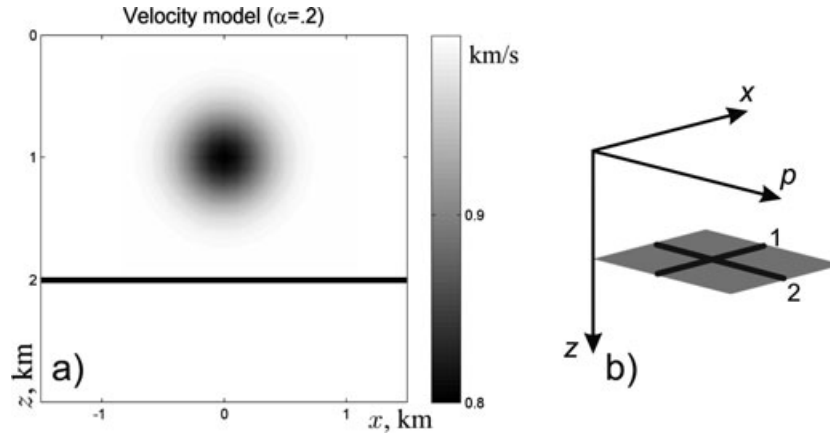


Figure 6. (a) The ‘true’ background velocity model (a low-velocity lens) and reflectivity function (reflector at $z = 2$); (b) diagram illustrating the presence of the reflector in $w_g = w_g(\alpha; z, x, p)$.

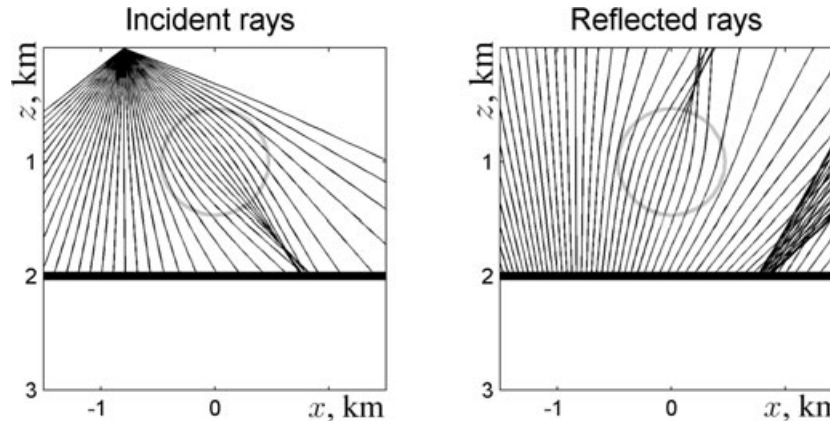


Figure 7. Incident and reflected rays for a single source. The lens in Fig. 6 (a) is, here, indicated by a grey circle. The rays are nowhere horizontal, while caustics are being formed.

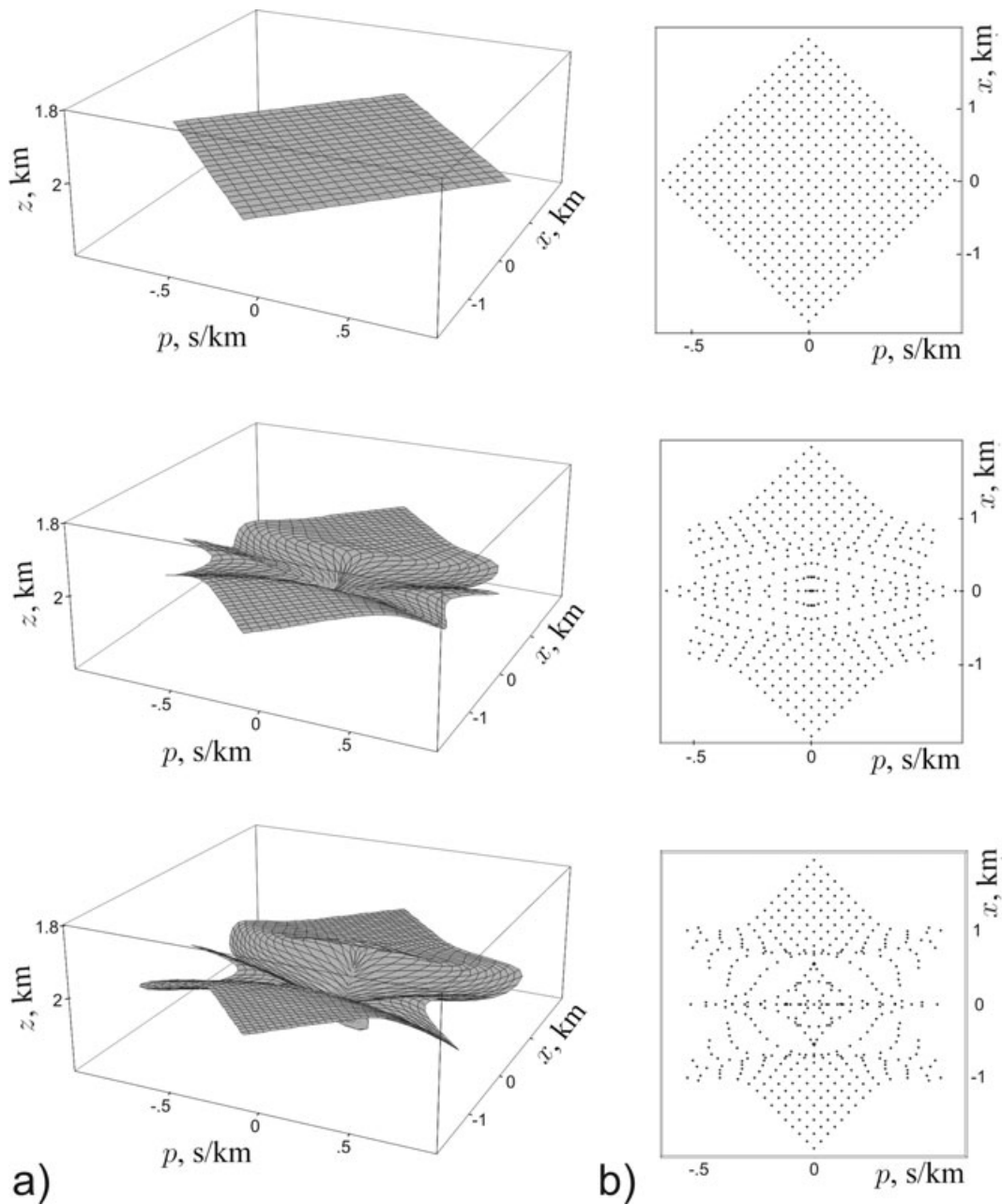


Figure 8. Velocity continuation of $w_g(\alpha; z, x, p)$, tracking the ‘front’ associated with the horizontal reflector shown in Fig. 6(a). (a) Continuation of the grey plane of Fig. 6(b), at $\alpha = 0.2$ (top), 0.1 (middle) and 0 (bottom); (b) a set of continuation rays: initial locations (top), endpoints at $\alpha = 0.1$ (middle) and endpoints at $\alpha = 0$ (bottom).

The evolution of a ‘front’ of $w_g(\alpha; z, x, p)$ with α is illustrated in Fig. 8(a) (top: $\alpha = 0.2$, that is the ‘true’ model; middle: $\alpha = 0.1$; and bottom: $\alpha = 0$, that is, the lens is absent). Due to restricted acquisition geometry (the sources and receivers are located within an interval $(-2, 2)$) we have illumination over a diamond-shaped region only (see Fig. 8a, b top). The dots in Fig. 8(b) top indicate the initial locations of a set of continuation rays; the dots in Fig. 8(b) middle, bottom, indicate the endpoints (at $\alpha = 0.1$ and $\alpha = 0$, respectively) of the continuation rays in this set, plotted in the (x, p) coordinate plane. We observe how the regularly spaced initial points evolve under velocity continuation, and their movement is not restricted to any coordinate plane. Indeed, MVA should not be carried out with separated common-image gathers.

However, due to the (common) symmetry of the background velocity models in our example, the velocity continuation of the $x = 0$ image gather takes place within the $x = 0$ plane (see Fig. 9 (right)). The velocity continuation of the image, at $p = 0$, stays within the $p = 0$ plane (see Fig. 9 (left)). In Fig. 9, we show the fronts (in the $x = 0$ and $p = 0$ planes, respectively), as thick lines, again, at $\alpha = 0.2$, 0.1 and 0 as well as the continuation (velocity) rays connecting them. As far as the image continuation, illustrated in Fig. 9 (left), is concerned, we notice the evolution towards an apparent structure of a syncline while underestimating the strength of the low velocity lens (a phenomenon that has been well recognized in seismic migration).

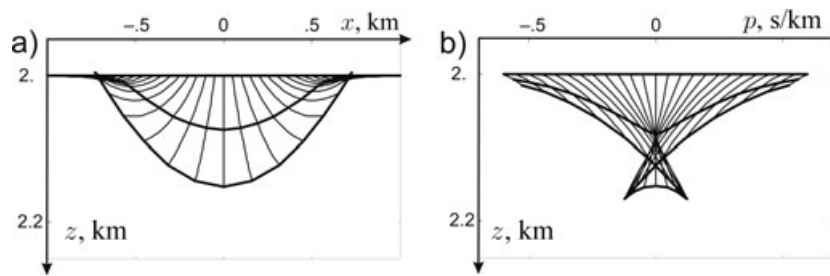


Figure 9. Continuation rays (thin lines) and ‘fronts’ at $\alpha = 0.2, 0.1$ and 0 (fat lines) under velocity continuation: (a) in the plane $p = 0$ (image plane) and in the $x = 0$ plane (image gather plane). These are sections of the volumes illustrated in Fig. 8.

We then use the same background model and reflector to illustrate velocity continuation of the extended image. In the ‘true’ model, the extended image is a line focused in (z, x, h) -space at subsurface offset $h = 0$. This line defocuses, while departing from the ‘true’ background model, following the fronts shown in Fig. 10.

8 EVOLUTION OPERATORS IN HOMOGENEOUS VELOCITY MODELS

In homogeneous velocity models ($c(z, x) = v$ independent of z and x) the evolution parameter becomes the velocity itself, $\alpha \equiv v$. The (principal) symbol of the DSR operator in (22) takes the form

$$P_1^{\text{DSR}}(v; z, s, r, \xi_s, \xi_r, \tau) = \tau \frac{1}{v^2 - \frac{\|\xi_s\|^2}{\tau^2}} + \tau \frac{1}{v^2 - \frac{\|\xi_r\|^2}{\tau^2}}, \quad (64)$$

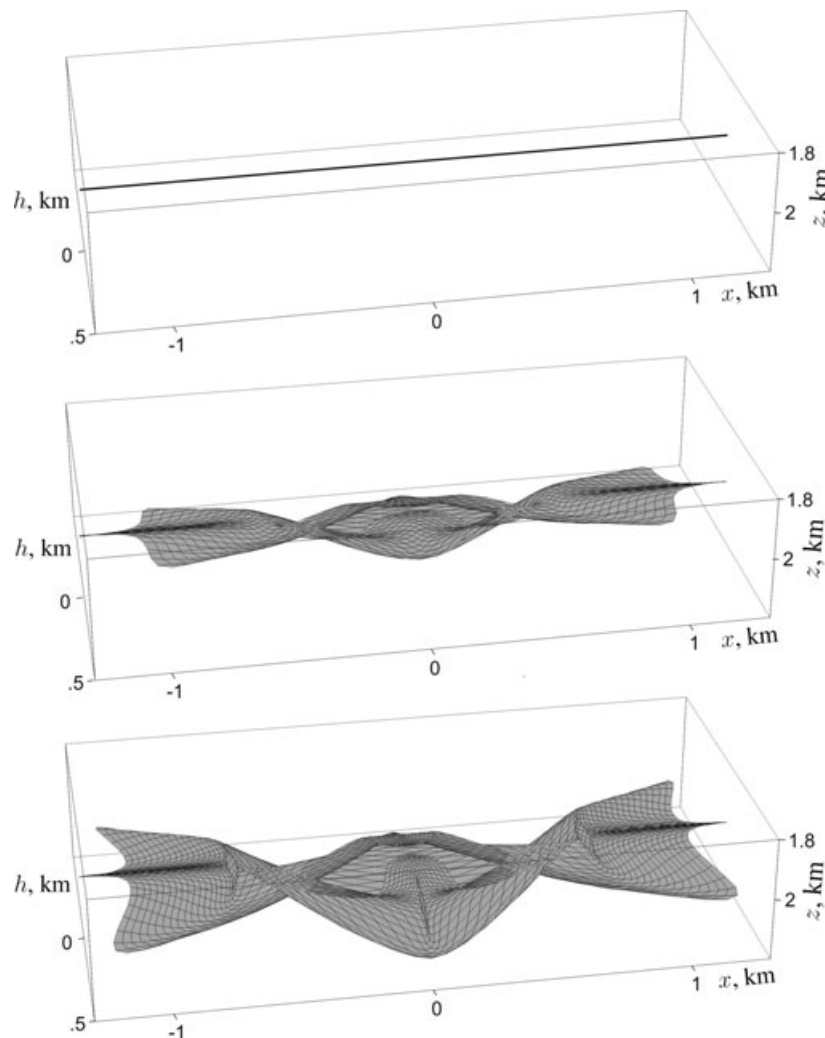


Figure 10. ‘Fronts’ following the velocity continuation of the extended image, $w_e(\alpha; z, x, h)$, of the horizontal reflector in the model illustrated in Fig. 6(a): at $\alpha = 0.2$ (a line representing the focusing at $h = 0$), 0.1 and 0 , signifying the gradual defocusing.

while the (principal) symbol in (23) becomes

$$\begin{aligned} \square_{\partial_v P^{\text{DSR}}_1}(v; z, s, r, \xi_s, \xi_r, \tau) &= -\mathbf{p} \frac{\tau}{v^{-2} - \|\xi_s\|^2/\tau^2} \frac{1}{v^3} - \mathbf{p} \frac{\tau}{v^{-2} - \|\xi_r\|^2/\tau^2} \frac{1}{v^3} \\ &= -\frac{1}{v^3} \mathbf{p} \frac{\xi_s}{v^{-2} - \|\xi_s\|^2/\tau^2} \mathbf{p} \frac{\xi_r}{v^{-2} - \|\xi_r\|^2/\tau^2}, \end{aligned} \quad (65)$$

using that $\mathbf{H}^{\text{DSR}}(z, s, r, t, \xi_z, \xi_s, \xi_r, \tau) = 0$, cf. (11). We derive, here, closed-form expressions for the evolution operators for velocity continuation of downward continued data, velocity continuation of extended images and velocity continuation of image gathers. We use these expressions to illustrate some of the features of these types of continuation that coexist in the data-extended-image volume.

Continuation of downward continued data. For the DSR rays corresponding to upward continuation operator $H_{(\bar{z}, z)}(v)$, we have

$$\Sigma_2(\bar{z}, z)(s, r, t, \xi_s, \xi_r, \tau) = (\xi_s, \xi_r, \tau),$$

that is, the wave numbers are preserved, which implies, with (65), that $(\partial_\alpha P^{\text{DSR}})_1(v; \bar{z}, \Sigma'(\bar{z}, z)(s, r, t, \xi_s, \xi_r, \tau))$ (cf. 29) is independent of \bar{z} . Evaluation of (30) then yields

$$P_1^d(v; z, s, r, \xi_s, \xi_r, \tau) = -\frac{\tau z}{v^3} \mathbf{p} \frac{1}{v^{-2} - \|\xi_s\|^2/\tau^2} + \mathbf{p} \frac{1}{v^{-2} - \|\xi_r\|^2/\tau^2}. \quad (66)$$

Extended image continuation. We get $\tau = \Theta^{-1}(v; z, s, r, \xi_z, \xi_s, \xi_r)$ directly from solving eq. ‘14’, subject to the substitution $c = v (= \alpha)$.

With this solution, we note that

$$\mathbf{p} \frac{1}{v^{-2} - \|\xi_s\|^2/\tau^2} = \frac{1}{2\xi_z} \square \xi_z^2 + \|\xi_r\|^2 - \|\xi_s\|^2 \square, \quad \mathbf{p} \frac{1}{v^{-2} - \|\xi_r\|^2/\tau^2} = \frac{1}{2\xi_z} \square \xi_z^2 + \|\xi_s\|^2 - \|\xi_r\|^2 \square. \quad (67)$$

Then, with (66) and (67), the evaluation of (45) yields

$$P_1^e(v; z, s, r, \xi_s, \xi_r, \xi_z) = -\frac{z}{v} \frac{\xi_z^4 + 2\xi_z^2 \|\xi_r\|^2 + \|\xi_s\|^2 \square + \|\xi_s\|^2 - \|\xi_r\|^2 \square}{\xi_z^4 - \|\xi_s\|^2 - \|\xi_r\|^2 \square}. \quad (68)$$

Applying coordinate transformation (16) results in

$$P_1^e(v; z, x, h, \xi_x, \xi_h, \xi_z) = -\frac{z}{v} \xi_z \frac{\xi_z^4 + \xi_z^2 \|\xi_x\|^2 + \|\xi_h\|^2 \square + \langle \xi_x, \xi_h \rangle^2}{\xi_z^4 - \langle \xi_x, \xi_h \rangle^2}. \quad (69)$$

REMARK (Stolt residual migration). Given the (principal) symbol, P_1^e , for extended image continuation, we obtain the Hamiltonian (cf. 5)

$$\mathbf{H}^e(v; z, s, r, \xi_v, \xi_z, \xi_s, \xi_r) = \xi_v - P_1^e(v; z, s, r, \xi_z, \xi_s, \xi_r), \quad (70)$$

which generates corresponding Hamilton eqs (6). With (68), these equations can be solved explicitly for given initial conditions $(z_0, s_0, r_0, \xi_{z0}, \xi_{s0}, \xi_{r0})$ (at $v = v_0$ say), resulting directly in the formulae for Stolt residual migration (Sava 2003; Stolt 1996). Note, however, that our Hamiltonian representation (68) and (69) is general, and allows different implementations in addition to, for example, the phase shift method (as discussed in Fomel (2003b)).

Continuation of common-image gathers. In homogeneous background velocity models, the symbol P_1^{DSR} is independent of s and r , whence the equations for (ξ_s, ξ_r, τ) in (50), given (ξ_z, ξ_x, ξ_p) , can be solved separately

$$\xi_s = \frac{1}{2}\xi_x + \tau p, \quad \xi_r = \frac{1}{2}\xi_x - \tau p, \quad \text{with } \tau^2 = \frac{\xi_z^2 v^2}{4} \frac{\xi_z^2 + \|\xi_x\|^2}{\xi_z^2(1 - \|vp\|^2) - \langle \xi_x, vp \rangle^2}; \quad (71)$$

these are all preserved under $\Sigma(z, 0)$. We then use the equations for (s, r) in (50), given (x, ξ_p) , to find s and r :

$$s = x - \frac{\xi_p}{2\tau}, \quad r = x + \frac{\xi_p}{2\tau}. \quad (72)$$

Eq. (51) yields

$$t = \tau^{-1} \langle p, \xi_p \rangle. \quad (73)$$

We immediately have obtained transformation $\tilde{\Sigma}$ in (57). Subjecting (66) to this transformation then yields

$$P_1^g(v; z, x, p, \xi_z, \xi_x, \xi_p) = -\frac{z}{v} \xi_z^3 \frac{\xi_z^2 + \|\xi_x\|^2}{\xi_z^4 - \xi_z^2 vp + \langle \xi_x, vp \rangle \xi_x}. \quad (74)$$

We obtain the Hamiltonian (cf. 5)

$$\mathbf{H}^g(v; z, x, p, \xi_v, \xi_z, \xi_x, \xi_p) = \xi_v - P_1^g(v; z, x, p, \xi_z, \xi_x, \xi_p), \quad (75)$$

which generates corresponding Hamilton eq. (6). The Hamiltonian for common-image gathers velocity continuation depends on (z, p) and v . In Fig. 11(a) we show the corresponding slowness surface, defined by $\mathbf{H}^g = 1$, using the notation $k_x = \xi_x/\xi_v$, $k_z = \xi_z/\xi_v$ and $k_p = \xi_p/\xi_v$. We set $z = 2$, $v = 1$ and $p = 0$ (outer cylindrical surface) and $p = 0.3$ (inner surface). From (74) and (75) it is clear that the slowness surface does not depend on k_p . This, in turn, means that the group velocity has no component in the direction of the p -axis, that is the energy flow, in the case of homogeneous media, stays within planes $p = \text{const}$. To illustrate this, we show a set of velocity rays in Fig. 11(b). Here, we

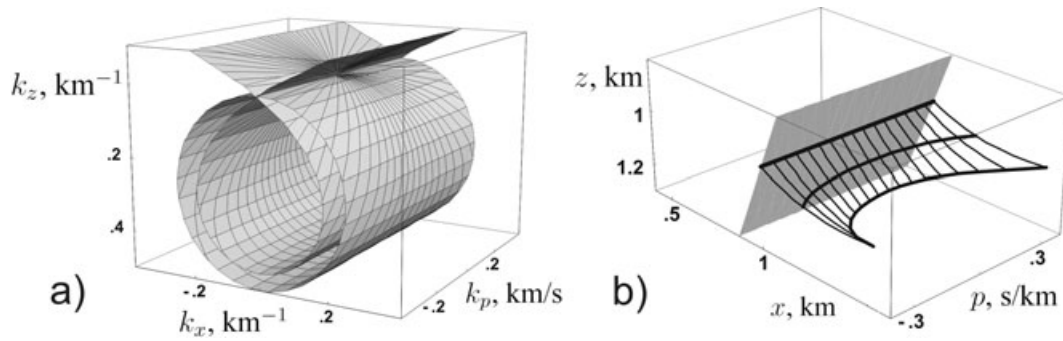


Figure 11. Velocity continuation of a common-image point gather in the case of homogeneous background velocities. (a) Slowness surface for the Hamiltonian in (75) for $v = 1$ and $p = 0$ (outer surface) and $p = 0.3$ (inner surface); (b) velocity continuation of a line in a common-image gather consisting of a dipping plane (in grey). Thin lines represent velocity rays, while the velocity is changing from a starting value $v = 1$ to $v = 1.2$. Three bold lines show the evolution of the straight line in the initial common-image gather (for $v = 1$) after velocity continuation to $v = 1.1$ and $v = 1.2$.

assume that initial common-image gather consists of a dipping plane in (z, x, p) -space (in grey). We then follow a transformation of one straight line in this plane ($x = z = 1$) under velocity continuation. Thin lines show velocity rays, while the velocity is changing from a starting value $v = 1$ to $v = 1.2$. Three bold lines show the evolution of the straight line in the initial common-image gather (for $v = 1$) after velocity continuation to $v = 1.1$ and $v = 1.2$.

9 DISCUSSION

We discuss our results in the context of implementational aspects using asymptotic ray theory. In the above, we have developed explicitly evolution equations for velocity continuation in the downward continuation (DSR) approach. The evaluation of the (principal) symbols of the evolution operators requires in principle retracing DSR rays (in phase space) in the evolving velocity models. However, the downward continuation of data needs not be repeated. Indeed, the data themselves are not directly involved in the process of velocity continuation proper.

Continuation operators are the solution operators of the mentioned evolution equations. In general these equations need to be solved numerically. Continuation operators propagate singularities along continuation rays, which are generated by Hamilton systems. Numerically solving these systems, in general, consists of two nested steps: Computing the Hamiltonians (and their derivatives), which involves a depth integration, followed by integrating the Hamilton systems. The complexity of numerically computing other continuation rays was recognized by (Adler 2002; Iversen 2004, 2006).

We showed that in a particular class of velocity models, admitting dependence in depth only, the retracing of DSR rays is unnecessary. In yet a different approach to velocity continuation, namely through so-called common reflection-point (CRP) stacks (Audebert *et al.* 1997) based on a class of velocity model perturbations of the type, $c(\alpha; z, x) = \alpha c_0(z, x)$, the ray geometry can be kept the same. However, unlike in our approach, the Kirchhoff summation has to be repeated for every α .

To allow for the occurrence of certain turning rays, it is possible to reformulate the downward continuation in curvilinear coordinates.

10 CONCLUSIONS

We developed a framework for velocity continuation in the downward continuation approach to seismic imaging. We based the framework on the DSR equation, and imposed the DSR assumption. In the process, it was then natural to introduce the concept of data-extended-image domain. Continuation takes place along curves in the space of allowable velocity models. As the main result, we obtained evolution equations for three interconnected velocity continuations: for downward continued data, (extended) images and common-image gathers formed from these. We used techniques from microlocal analysis, in particular, Egorov's theorem.

The numerical solution of the evolution equation for continuation can be constructed as follows. The initial values (downward continued data, image or image gathers) can be decomposed into curvelets or wave packets and subsequently compressed (Candès & Donoho 2005a,b; Duchkov *et al.* 2008b). Then the solution of the evolution can be efficiently computed with curvelets (see Andersson *et al.* 2008). To leading order, the curvelets that appear in the decomposition of the initial values are subjected to a 'flow-out' (Douma & De Hoop 2007; De Hoop *et al.* 2008) following the continuation 'rays' in phase space. Moreover, the number of rays to be retraced in computing the evolution operator reduces with the rate of compression. Continuation can be viewed as an alternative to (map) remigrating curvelets that appear in the decomposition of surface reflection data (Douma & De Hoop 2007).

We derived explicit formulae for the evolution operators in the case of special background velocity models: In the case of models with a linear velocity growth with depth (the evolution parameter is the gradient) for the continuation of extended images, and in the case of homogeneous velocity models (the evolution parameter is the velocity itself) for the continuation of extended images and common-image gathers. Formulae for common-image gathers continuation are new, while other results reproduce earlier work by (Fomel 1994; Fomel 2003a; Sava 2003). Though not applicable to generic situations, these formulae provide some insight also in connection with the history of residual

velocity (poststack) migration (e.g. Stolt 1996). Formulae derived in the homogeneous case have been used for the class of velocity model perturbations, $c(\alpha; z, x) = \alpha c_0(z, x)$, to implement ‘approximate’ residual pre-stack Stolt migration in Sava & Biondi (2004).

We present a 2-D synthetic data example for the velocity continuation of the extended image and common-image gathers associated with a plane horizontal reflector in a family of background models with a low-velocity lens that varies in strength. Thus we illustrate velocity continuation in the presence of caustics.

ACKNOWLEDGMENTS

The authors would like to thank Sergey Fomel and an unknown reviewer for many valuable comments that helped improving the paper. This research was funded in part by NSF CMG grant EAR-0417891. The authors also thank the members, BP, ConocoPhillips, ExxonMobil, StatoilHydro and Total, of the Geo-Mathematical Imaging Group for financial support.

REFERENCES

- Adler, F., 2002. Kirchhoff image propagation, *Geophysics*, **67**, 126–134.
- Andersson, F., De Hoop, M., Smith, H. & Uhlmann, G., 2008. A multi-scale approach to hyperbolic evolution equations with limited smoothness, *Commun. Part. Diff. Eq.*, **33**, 988–1017.
- Audebert, F., Diet, J., Guillaume, P., Jones, I.F. & Zhang, X., 1997. CRP-scans: 3-D preSDM velocity analysis via zero-offset tomographic inversion, in *Proceedings of the 67th Annual International Meeting: Expanded Abstracts, SEG*, Tulsa, pp. 1805–1808.
- Belonosova, A. & Alekseev, A., 1967. About one formulation of the inverse kinematic problem of seismics for a two-dimensional continuously heterogeneous medium, in *Some Methods and Algorithms for Interpretation of Geophysical Data (in Russian)*, pp. 137–154, ed. M.M. Lavrentiev, Nauka, Moscow.
- Biondi, B., 2006. *3D Seismic Imaging*, Vol. 14, Investigations in Geophysics Series, SEG, Tulsa, OK.
- Candès, E. & Donoho, D., 2005a. Continuous curvelet transform: I. Resolution of the wavefront set, *Appl. Comput. Harmonic Anal.*, **19**, 162–197.
- Candès, E. & Donoho, D., 2005b. Continuous curvelet transform: II. Discretization and frames, *Appl. Comput. Harmonic Anal.*, **19**, 198–222.
- Claerbout, J., 1985. *Imaging the Earth's Interior*, Blackwell Scientific Publishing, Oxford.
- Claerbout, J., 1986. Velocity extrapolation by cascaded 15 degree migration, Stanford University (Technical Report SEP-48), pp. 79–84.
- Clayton, R., 1978. Common midpoint migration, Stanford University, (Technical Report, SEP-14).
- De Hoop, M., Le Rousseau, J. & Biondi, B., 2003. Symplectic structure of wave-equation imaging: a path-integral approach based on the double-square-root equation, *Geophys. J. Int.*, **153**, 52–74.
- De Hoop, M., Smith, H., G., U. & van der Hilst, R., 2008. Seismic imaging with the generalized radon transform: a curvelet transform perspective, *Inv. Prob.*, in press.
- De Hoop, M., Van der Hilst, R. & Shen, P., 2006. Wave-equation reflection tomography: annihilators and sensitivity kernels, *Geophys. J. Int.*, **167**, 1332–1352.
- Douma, H. & De Hoop, M., 2007. Leading-order seismic imaging using curvelets, *Geophysics*, **72**, S231–S248.
- Duchkov, A., De Hoop, M. & Sá Barreto, A., 2008a. Evolution-equation approach to seismic image, and data, continuation, *Wave Motion*, **45**, 952–969.
- Duchkov, A., Andersson, F. & De Hoop, M., 2008b. Discrete, almost symmetric wave packets and higher-dimensional ‘curvelet’ transform in seismology, *J. Comput. Phys.*, submitted.
- Etgen, J., 1990. Residual prestack migration and interval velocity estimation, *PhD thesis*, Stanford University, CA.
- Farra, V., 1999. Computation of second-order traveltime perturbation by Hamiltonian ray theory, *Geophys. J. Int.*, **136**, 205–217.
- Fishman, L. & McCoy, J., 1984a. Derivation and application of extended parabolic wave theories I. The factorized Helmholtz equation, *J. Math. Phys.*, **25**, 285–296.
- Fishman, L. & McCoy, J., 1984b. Derivation and application of extended parabolic wave theories II. Path integral representations, *J. Math. Phys.*, **25**, 297–308.
- Fomel, S., 1994. Method of velocity continuation in the problem of seismic time migration, *Russ. Geol. Geophys.*, **35**(5), 100–111.
- Fomel, S., 2003a. Velocity continuation and the anatomy of residual prestack time migration, *Geophysics*, **68**, 1650–1661.
- Fomel, S., 2003b. Time-migration velocity analysis by velocity continuation, *Geophysics*, **68**, 1662–1672.
- Foster, D., Mosher, C. & Jin, S., 2002. Offset plane wave migration, in *Expanded Abstracts*, pp. B–14, Eur. Assoc. Expl. Geophys.
- Goldin, S., 1994. Superposition and continuation of operators used in seismic imaging, *Russ. Geol. Geophys.*, **35**(9), 131–145.
- Goldin, S., 1998. Geometric fundamentals of seismic imaging: a geometric theory of the upper level, in *Amplitude-preserving seismic reflection imaging*, in *Proceedings of the Workshop*, pp. 120–223, Geophysical Press, London.
- Goldin, S., 2003. Geometrical fundamentals of seismic imaging: realization of contact mappings, *Siberian J. Numer. Math.*, **6**(4), 323–345.
- Hubral, P., Tygel, M. & Schleicher, J., 1996. Seismic image waves, *Geophys. J. Int.*, **125**, 431–442.
- Iversen, E., 1996. Derivatives of reflection point coordinates with respect to model parameters, *Pure appl. Geophys.*, **148**, 287–317.
- Iversen, E., 2004. The isochron ray in seismic modeling and imaging, *Geophysics*, **69**, 1053–1070.
- Iversen, E., 2006. Velocity rays for heterogeneous anisotropic media: theory and implementation, *Geophysics*, **71**, T117–T127.
- Liu, H. & McMechan, G., 1996. Dynamic residual prestack depth migration for common offset gathers, in *Report*, University of Texas at Dallas.
- Loris, I., Nolet, G., Daubechies, I. & Dahlen, F., 2007. Tomographic inversion using ℓ^1 -norm regularization of wavelet coefficients, *Geophys. J. Int.*, **170**, 359–370.
- Mosher, C., Foster, D. & Hassanzadeh, S., 1996. Seismic imaging with offset plane waves, in *Mathematical Methods in Geophysical Imaging IV, Proceedings of SPIE Volume 2822*, pp. 52–63.
- Sava, P., 2003. Prestack residual migration in the frequency domain, *Geophysics*, **68**, 634–640.
- Sava, P. & Biondi, B., 2004. Wave-equation migration velocity analysis. I. Theory, *Geophys. Prospect.*, **52**, 593–606.
- Shen, P., 2004. Automatic wave equation migration velocity analysis using differential semblance, *PhD thesis*, Rice University.
- Stolk, C. & De Hoop, M., 2001. Seismic inverse scattering in the ‘wave-equation’ approach, *MSRI preprint*, #2001–047.
- Stolk, C. & De Hoop, M., 2005. Modeling of seismic data in the downward continuation approach, *SIAM J. Appl. Math.*, **65**, 1388–1406.
- Stolk, C. & De Hoop, M., 2006. Seismic inverse scattering in the downward continuation approach, *Wave Motion*, **43**, 579–598.
- Stolt, R., 1996. Short note—a prestack residual time migration operator, *Geophysics*, **61**, 605–607.
- Symes, W. & Carazzone, J., 1991. Velocity inversion by differential semblance optimization, *Geophysics*, **56**, 654–663.
- Treves, F., 1980. *Introduction to Pseudodifferential and Fourier Integral Operators*, Vol. 2, Plenum Press, New York.
- Tygel, M., Schleicher, J. & Hubral, P., 1996. A unified approach to 3-D seismic reflection imaging, Part II: theory, *Geophysics*, **61**, 759–775.

APPENDIX A: EGOROV'S THEOREM

A precise formulation of Egorov's theorem can be found in (Treves 1980, theorem 6.2). Here, we provide an intuitive understanding of this theorem with a view to applications in seismic wave-equation imaging.

We consider an invertible Fourier integral operator, F say, the canonical relation of which is the graph of a transformation Σ . Suppose $F : E'(Y) \rightarrow D'(X)$; F propagates singularities according to $(y, \eta) \rightarrow (x, \xi) = \Sigma(y, \eta)$. An example is F^{-1} being common-offset Kirchhoff migration (absence of caustics) and Σ describing map demigration.

We then consider a pseudodifferential operator, P , with principal symbol $P_1 = P_1(x, \xi)$. The operator $Q = F^{-1}PF$ is also a pseudodifferential operator. Its principal symbol, $Q_1 = Q_1(y, \eta)$, is given by

$$Q_1(y, \eta) = P_1(\Sigma(y, \eta)). \quad (\text{A1})$$

In the main text, we repeatedly arrange operators such that the theorem can be applied.

APPENDIX B: VERTICALLY INHOMOGENEOUS BACKGROUND VELOCITY MODELS

Retracing rays and perturbation theory *are not required* for velocity continuation in the case of a family of vertically inhomogeneous background velocities, $c(\alpha; z)$. Then H^{DSR} does not depend on s, r (and t) so that $\partial_{(s,r,t)} H^{\text{DSR}} = 0$ and ξ_s, ξ_r and τ are constant along DSR rays in phase space. Formulae (23) and (30) simplify according to

$$\partial_\alpha P^{\text{DSR}}_1(\alpha; z, s, r, \xi_s, \xi_r, \tau) = -\frac{\partial_\alpha c}{c^3}(\alpha; z) \left(\frac{\tau}{c(\alpha; z)^{-2} - \|\xi_s\|^2/\tau^2} + \frac{\tau}{c(\alpha; z)^{-2} - \|\xi_r\|^2/\tau^2} \right), \quad (\text{B1})$$

and

$$P^d_1(\alpha; z, s, r, \xi_s, \xi_r, \tau) = -\frac{\partial_\alpha c}{c^3}(\alpha; \bar{z}) \left(\frac{\tau}{c(\alpha; \bar{z})^{-2} - \|\xi_s\|^2/\tau^2} + \frac{\tau}{c(\alpha; \bar{z})^{-2} - \|\xi_r\|^2/\tau^2} \right) d\bar{z}, \quad (\text{B2})$$

respectively. Moreover, we obtain

$$\Theta^{-1}(z, s, r, \xi_s, \xi_r) = \frac{c(\alpha; z)}{2\xi_z} \left(\frac{1}{(\|\xi_s\| - \|\xi_r\|)^2 + \xi_z^2} - \frac{1}{(\|\xi_s\| + \|\xi_r\|)^2 + \xi_z^2} \right), \quad (\text{B3})$$

which, upon substitution for τ in (B2), gives us $P^e_1(\alpha; z, s, r, \xi_s, \xi_r)$ for velocity continuation of extended images, cf. (45). Clearly, no DSR rays have to be traced.

For some particular choices of families $c(\alpha; z)$, it is possible to carry out the integration on the right-hand side of (B2) in a closed form. For example, if $c(\alpha; z) = c_0 + \alpha z$, we get:

$$P^d_1(\alpha; z, s, r, \xi_s, \xi_r, \tau) = -\frac{1}{\alpha^2} c_0(q_s + q_r) - \frac{\tau}{\alpha^2} \log \left(4\alpha^4 q_s + \frac{\tau}{c_0 + \alpha \bar{z}} q_r + \frac{\tau}{c_0 + \alpha \bar{z}} \right), \quad (\text{B4})$$

where $q_r = \tau \frac{1}{(c_0 + \alpha \bar{z})^{-2} - \|\xi_r\|^2/\tau^2}$, $q_s = \tau \frac{1}{(c_0 + \alpha \bar{z})^{-2} - \|\xi_s\|^2/\tau^2}$.